# Scattering suppression in epsilon-near-zero plasmonic fractal shells

**Vashista C. de Silva,[1] Piotr Nyga,[2] and Vladimir P. Drachev[1,*]**

[1]*University of North Texas, Department of Physics and Center for Advanced Research and Technology, 1155 Union Circle, Denton, TX 76203, USA*

[2]*Institute of Optoelectronics, Military University of Technology, 2 Kaliskiego Str., 00-908 Warsaw, Poland*

[*]*vladimir.drachev@unt.edu*

**Abstract:** Significant extinction from the visible to mid-infrared makes fractal shells very attractive as aerosolized obscurants. In contrast to the planar fractal films, where the absorption and reflection equally contribute to the extinction, the shells' extinction is caused mainly by the absorption. The Mie scattering resonance at 560 nm of a silica core with 780 nm diameter is suppressed by 75% and only partially substituted by the absorption in the shell so that the total transmission is noticeably increased. The silica vibrational stretching band at 9 μm in absorption also disappears. Effective medium theory supports our experiments and indicates that light goes mostly through the epsilon-near-zero shell with approximately wavelength independent absorption rate.



**OCIS codes:** (160.4236) Nanomaterials; (290.5839) Scattering, invisibility; (240.6680) Surface plasmons; (290.5820) Scattering measurements; (220.4241) Nanostructure fabrication; (290.1090) Aerosol and cloud effects.

## References and links

1. A. L. Aden and M. Kerker, "Scattering of electromagnetic waves from two concentric spheres," J. Appl. Phys. **22**(10), 1242–1246 (1951).
2. M. Kerker, "Invisible bodies," J. Opt. Soc. Am. **65**(4), 376–379 (1975).
3. H. Chew and M. Kerker, "Abnormally low electromagnetic scattering cross sections," J. Opt. Soc. Am. **66**(5), 445–449 (1976).
4. A. Alù and N. Engheta, "Achieving transparency with plasmonic and metamaterial coatings," Phys. Rev. E Stat. Nonlin. Soft Matter Phys. **72**(1), 016623 (2005).
5. M. G. Silveirinha, A. Alù, and N. Engheta, "Parallel-plate metamaterials for cloaking structures," Phys. Rev. E Stat. Nonlin. Soft Matter Phys. **75**(3), 036603 (2007).
6. S. Oldenburg, R. Averitt, S. Westcott, and N. Halas, "Nanoengineering of optical resonances," Chem. Phys. Lett. **288**(2–4), 243–247 (1998).
7. F. Tam, A. L. Chen, J. Kundu, H. Wang, and N. J. Halas, "Mesoscopic nanoshells: geometry-dependent plasmon resonances beyond the quasistatic limit," J. Chem. Phys. **127**(20), 204703 (2007).
8. C. Graf and A. van Blaaderen, "Metallodielectric colloidal core–shell particles for photonic applications," Langmuir **18**(2), 524–534 (2002).
9. T. Ji, V. G. Lirtsman, Y. Avny, and D. Davidov, "Preparation, characterization, and application of Au-shell/polystyrene beads and Au-shell/magnetic beads," Adv. Mater. **13**(16), 1253–1256 (2001).
10. C. A. Rohde, K. Hasegawa, and M. Deutsch, "Coherent light scattering from semicontinuous silver nanoshells near the percolation threshold," Phys. Rev. Lett. **96**(4), 045503 (2006).
11. D. Stauffer, *Introduction to Percolation Theory* (CRC Press, 1994).
12. Y. Yagil, M. Yosefin, D. J. Bergman, G. Deutscher, and P. Gadenne, "Scaling theory for the optical properties of semicontinuous metal films," Phys. Rev. B Condens. Matter **43**(13), 11342–11352 (1991).
13. Y. Yagil, P. Gadenne, C. Julien, and G. Deutscher, "Optical properties of thin semicontinuous gold films over a wavelength range of 2.5 to 500 μm," Phys. Rev. B Condens. Matter **46**(4), 2503–2511 (1992).
14. M. I. Stockman, L. N. Pandey, L. S. Muratov, and T. F. George, "Comment on "Photon scanning tunneling microscopy images of optical excitations of fractal metal colloid clusters"," Phys. Rev. Lett. **75**(12), 2450 (1995).
15. M. I. Stockman, L. N. Pandey, L. S. Muratov, and T. F. George, "Optical absorption and localization of eigenmodes in disordered clusters," Phys. Rev. B Condens. Matter **51**(1), 185–195 (1995).
16. M. I. Stockman, L. N. Pandey, and T. F. George, "Inhomogeneous localization of polar eigenmodes in fractals," Phys. Rev. B Condens. Matter **53**(5), 2183–2186 (1996).

#250070 Received 14 Sep 2015; revised 8 Oct 2015; accepted 8 Oct 2015; published 12 Oct 2015

17. M. I. Stockman, "Inhomogeneous eigenmode localization, chaos, and correlations in large disordered clusters," Phys. Rev. E Stat. Phys. Plasmas Fluids Relat. Interdiscip. Topics **56**(6), 6494–6507 (1997).
18. S. Grésillon, L. Aigouy, A. Boccara, J. Rivoal, X. Quelin, C. Desmarest, P. Gadenne, V. Shubin, A. Sarychev, and V. Shalaev, "Experimental observation of localized optical excitations in random metal-dielectric films," Phys. Rev. Lett. **82**(22), 4520–4523 (1999).
19. D. A. Genov, A. K. Sarychev, and V. M. Shalaev, "Metal-dielectric composite filters with controlled spectral windows of transparency," J. Nonlinear Opt. Phys. Mater. **12**(4), 419–440 (2003).
20. P. Nyga, V. P. Drachev, M. D. Thoreson, and V. M. Shalaev, "Mid-IR plasmonics and photomodification with Ag films," Appl. Phys. B **93**(1), 59–68 (2008).
21. M. D. Thoreson, J. Fang, A. V. Kildishev, L. J. Prokopeva, P. Nyga, U. K. Chettiar, V. M. Shalaev, and V. P. Drachev, "Fabrication and realistic modeling of three-dimensional metal-dielectric composites," J. Nanophotonics **5**(1), 051513 (2011).
22. A. K. Sarychev and V. M. Shalaev, *Electrodynamics of Metamaterials* (World Scientific, 2007).
23. D. A. G. Bruggeman, "Berechnung verschiedener physikalischer konstanten von heterogenen substanzen," Ann. Phys. **416**(7), 636–664 (1935).
24. T. Pham, J. B. Jackson, N. J. Halas, and T. R. Lee, "Preparation and characterization of gold nanoshells coated with self-assembled monolayers," Langmuir **18**(12), 4915–4920 (2002).
25. Application note, "*Applications and Use of Integrating Spheres*," (PerkinElmer Inc., 2004), http://www.perkinelmer.com/CMSResources/Images/44-74191APP_LAMBDA650IntegratingSpheres.pdf
26. A. L. Smith, "Infrared Spectra-Structure Correlations for Organosilicon Compounds," Spectrochim. Acta **16**(1–2), 87–105 (1960).
27. C. F. Bohren and D. R. Huffman, *Absorption and Scattering of Light by Small Particles* (John Wiley & Sons, Inc., 1983).
28. I. Malitson, "Interspecimen comparison of the refractive index of fused silica," J. Opt. Soc. Am. **55**(10), 1205–1208 (1965).
29. T. R. Steyer, K. L. Day, and D. R. Huffman, "Infrared absorption by small amorphous quartz spheres," Appl. Opt. **13**(7), 1586–1590 (1974).
30. P. B. Johnson and R. W. Christy, "Optical Constants of the Noble Metals," Phys. Rev. B **6**(12), 4370–4379 (1972).
31. K. P. Chen, V. P. Drachev, J. D. Borneman, A. V. Kildishev, and V. M. Shalaev, "Drude relaxation rate in grained gold nanoantennas," Nano Lett. **10**(3), 916–922 (2010).
32. G. P. Motulevich, *Optical Properties of Metals* (Consultants Bureau, 1973).
33. Z. S. Wu, L. X. Guo, K. F. Ren, G. Gouesbet, and G. Gréhan, "Improved algorithm for electromagnetic scattering of plane waves and shaped beams by multilayered spheres," Appl. Opt. **36**(21), 5188–5198 (1997).

## 1. Introduction

Light scattering by core-shell particles made of dielectric and metal, manifests in a variety of phenomena predicted many decades ago [1–3]. The scattering suppression for coated confocal ellipsoids was introduced by Aden and Kerker [1–3] in the approximation of long wavelength planar electromagnetic waves. The authors called this scattering suppression - "invisibility". In the core-shell spheres, total sizes could be up to one fifth of the wavelength to achieve sensible invisibility for planar electromagnetic waves [4,5]. In this case, the wave can penetrate through the shell and the effect is associated with the out-of-phase scattering properties of plasmonic materials and the dielectric core. By varying the relative dimensions of the dielectric core and high quality continuous metal shell, the sharp optical resonances of these nanoparticles can be varied over hundreds of nanometers in wavelength, across the visible and into the infrared region of the spectrum [6,7]. In contrast, semicontinuous shells provide broadband response similar to the planar semicontinuous films, as it was shown for the visible spectral range [8–10]. The optical properties of the metal-dielectric semicontinuous films are influenced by multiple surface plasmon resonances (SPRs) in metal nanostructures, accumulating and building up electromagnetic energy in a broad spectral range at the nanometer scale [11–22]. A universal phenomenon in the localization of optical energy in inhomogeneous plasmonic media is the formation of hot spots, spatially fluctuating field with spikes in nanometer-size regions determined by the minimum scale of the nanoplasmonic system [14,15]. The picture of nanolocalization of the optical energy in disordered clusters is called inhomogeneous localization [16,17] assuming that there are different plasmonic eigenmodes, which coexist at close frequencies and have completely different localization sizes, ranging from the minimum scale to the scale of the entire systems. Each eigenmode may consist of a different number of sharp hot spots. Note that such type of

#250070 Received 14 Sep 2015; revised 8 Oct 2015; accepted 8 Oct 2015; published 12 Oct 2015

disordered geometry has typically fractal dimensions [12,13]. As it is known for the planar fractal films, the critical value of the metal coverage, called percolation threshold [11] results in a variety of plasmon resonances covering a spectral range from the visible to infrared. Thus the fractal films being synthesized on the microspheres can be promising aerosolized obscurants in the extremely broad visible-infrared spectral range.

Here we study silica-gold core-shell microspheres with plasmonic fractal shells. The similarities and differences with the planar noble metal fractal films have been experimentally established, which were not addressed in the earlier publications [8–10]. We show that the forward scattering of the silica microspheres is strongly suppressed. Also the reflection of the fractal shells does not grow with coverage approaching the percolation threshold. This is in contrast to the planar fractal films, where the forward scattering reduces along with the backscattering increasing as the metal coverage increases. Even more counterintuitive result is that the total extinction of the core-shell is decreased relative to the bare core response. The system is simulated using Mie theory with Aden and Kerker extension [1]. The fractal shell parameters are calculated with the Bruggeman effective medium theory (EMT) [23]. We discuss the EMT results and its applicability using the scaling theory approach [12,13]. The model provides a reasonable agreement with experiments in the broad spectral range, from 400 nm to 20 μm , covering shorter and longer wavelengths relative to the microsphere size. Both experiments and simulations show that the fractal shell with metal filling factor close to 0.5 enables scattering suppression in the visible range along with the increase in total transmission at the wavelength of Mie scattering peak at about 560 nm. The results indicate that this suppression is not just a spectral shift of the resonance in scattering, but suppression of its amplitude without noticeable shift. In the infrared range the gold semicontinuous shell "hides" the absorption resonance of the silica sphere at 9 μm . The effective permittivity for our samples is shown to be epsilon-near-zero for the real part $\varepsilon'$ . The imaginary epsilon multiplied by the frequency $\omega\varepsilon''$ approximately does not depend on the wavelength across the broad spectral range 0.5-20 μm .

## 2. Results and discussion

In the experiments, silica microspheres with a diameter of about 780 nm were coated with gold nanostructures using a modified method of the reduction of gold salt, chloroauric acid ($HAuCl_4$) with formaldehyde ($CH_2O$) in the presence of surfactants and stabilizers, initially developed for continuous shells [24]. The recipe was modified in order to fabricate semicontinuous shells. Specifically the gold reduction with formaldehyde was directly performed on the amino functionalized silica microspheres without preliminary seeding. The surface coverage of the gold on the microsphere surface was varied for different samples by varying the reduction time. The solution was stabilized with polyvinylpyrrolidone (PVP) to prevent aggregation of the microspheres. The Methods section provides more details. The synthesized gold-coated microspheres were deposited on zinc selenide (ZnSe) substrates for the infrared spectroscopy and on fused silica substrates for spectroscopy in the visible range [25].

Several different samples have been synthesized to study the effect of the shell structures with gradually increasing gold coverage (p). The spectra for normalized extinction (NE) are presented in Fig. 1. The normalized transmittance (NT) spectra were first normalized by the transmittance of the bare substrate. Since the density of microspheres on substrate was slightly different for different samples the extinction was normalized per the density. The normalized extinction spectra were calculated as $\mathrm{NE}=\left(-\log \mathrm{NT}\right)/\mathrm{N_S}$ , where $\mathrm{N_S}$ is the core-shell microsphere surface density calculated from the field emission scanning electron microscopy (FESEM) images and taken in $\mu\mathrm{m}^{-2}$ , and is presented in Table 1. FESEM images of different shell structures corresponding to the normalized extinction spectra are presented

#250070 Received 14 Sep 2015; revised 8 Oct 2015; accepted 8 Oct 2015; published 12 Oct 2015

in Fig. 2. The samples are labeled from 0 to 4, where 0 corresponds to the sample of bare silica microspheres ($p_0 = 0$) and 1-4 correspond to the samples with gradually increasing gold coverage in the shells, namely $p_1 = 0.38 \pm 0.03$, $p_2 = 0.47 \pm 0.01$, $p_3 = 0.58 \pm 0.03$, and $p_4 = 0.85 \pm 0.02$. Note that the FESEM images allow to measure only 2D projection of the structure and the gold coverage is calculated for such a plane view. That is a good approximation of the resulting filling fraction of metal (f) which we use in the simulations for less dense shells. The samples 3 and 4 can be clearly seen as having 3D structure, and thus the filling fraction can be less than estimated from the plane coverage. The shells have the fractal structure with fractal dimension D = 1.75-1.82 (see Table 1). It was calculated as the power dependence of the number of gold nanoparticles $N_p$ inside the circle of radius R, $N_p/N_0 = (R/R_0)^D$ [12]. For the bare silica microspheres there is the absorption peak due to the Si-O-Si vibrational stretching band at 9 μm [26] and there is an extinction peak in the visible spectral range due to the Mie scattering resonance at 560 nm (Fig. 1 for p = 0).

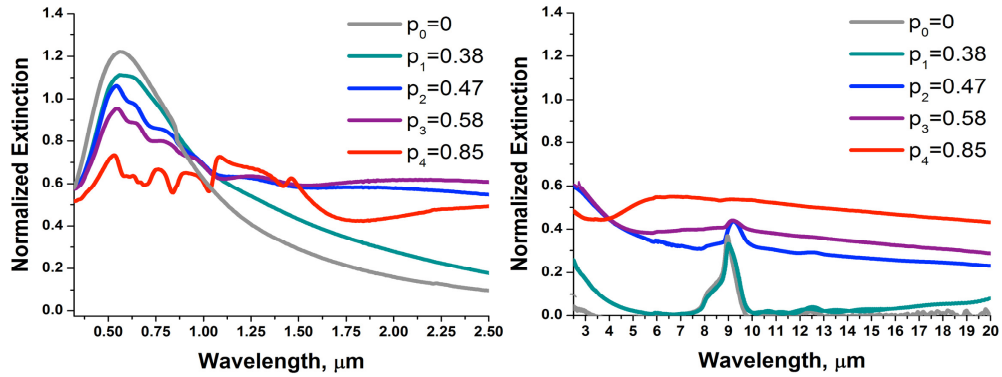


Fig. 1. Normalized extinction spectra of the core-shell particles with different gold shell coverage and morphologies shown in Fig. 2.

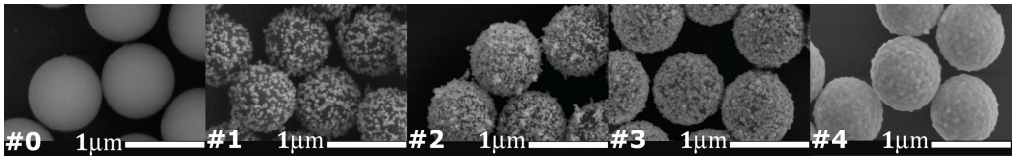


Fig. 2. FESEM images of the core-shell particles with different gold shell coverage and morphologies.

The spectra in Fig. 1 show strong dependence on the shell structure. The extinction spectra become broadband and spread out from the visible to infrared as the coverage increases. Note that this feature looks similar to the planar semicontinuous films, where the broadening of extinction spectra has been theoretically and experimentally demonstrated near the percolation threshold [12–22]. The critical feature of the semicontinuous films is the enhanced absorption at the range of the surface coverage, measured as the relative deviation from the percolation $\delta p = (p - p_c)/p_c$, between 0.2 and −0.2, where $p_c = 0.68$ [12]. The shell structure of the sample "1" is composed mainly of small Au fractals, most of which are isolated. The deviation $\delta p_1 = -0.44$ and, consequently, the extinction does not increase much for longer wavelengths as similar to the planar films. As soon as the relative deviation $\delta p$ becomes inside the critical range, as for sample "3", the extinction increases in the near- and mid-infrared regions. The extinction increases for both below and above the Si-O-Si vibration band for this shell structure. The extinction of bare $SiO_2$ sphere at the position of the Si-O-Si vibration band is caused mainly by the absorption in silica and scattering does not

#250070 Received 14 Sep 2015; revised 8 Oct 2015; accepted 8 Oct 2015; published 12 Oct 2015

have a major effect [26]. By keeping the shell thickness relatively constant and increasing the metal filling fraction from sample 2 to sample 4, the extinction is gradually increased. One can see in Fig. 1 that the broadening occurs for the samples "2"-"4". Surprisingly, it completely hides the absorption of the silica vibration band at 9 μm. Note that since silica microspheres have very low absorption in the visible, the extinction from bare silica particles is purely due to the scattering. As the gold coverage of the shell structure increases creating gold fractals, the extinction decreases. The scattering peak at 560 nm is suppressed and substituted by absorption in the shell at the lower level, so that the total transmission is increased. Indeed one can see that the absorption in the visible range is almost independent on the wavelength. It allows one to estimate the magnitude of the absorption at 560 nm and confirms that scattering is significantly suppressed.

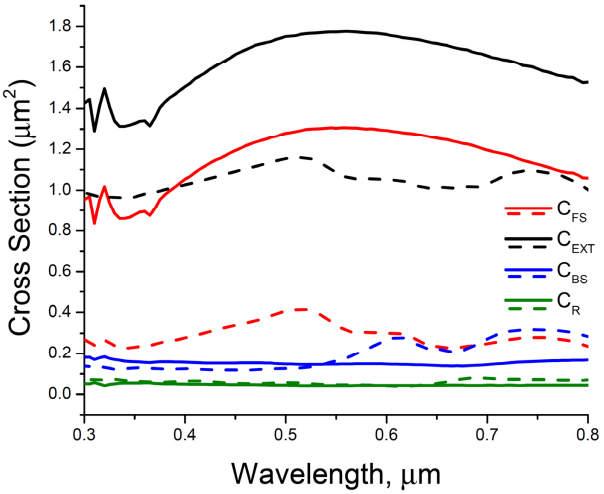


Fig. 3. Measured cross sections, $C_{FS}$, $C_{EXT}$, $C_{BS}$, and $C_R$ spectra of a submonolayer of bare silica microspheres "0" (solid lines) and gold-coated silica microspheres "4" (dashed lines).

Detailed measurements with the integrating sphere allow obtaining contributions of both scattering and absorption. The core-shell optical studies are typically limited to the extinction. However the scattering measurements give important details of the core-shell optics. The transmittance (T), specular reflectance (R), and forward- (FS) and back-scattering (BS) spectra were collected for bare silica and gold-coated silica microspheres, i.e. sample "0" with p = 0 and sample "4" with p = 0.85. The spectra were collected with the integrating sphere accessory [25]. The transmittance was measured along the optical axis of the integrating sphere; forward scattering occurred in the forward semi sphere and excludes light transmitted along the axis; the specular reflectance was measured as the reflected light with incidence angle of 8 degrees; backscattering occurred in the backward semi sphere and excludes specular reflection. All the spectra are normalized per particle surface density ( $N_S$ ), 0.4 $\mu m^{-2}$ for bare microspheres and 0.5 $\mu m^{-2}$ for core-shell sample "4". The results are plotted in Fig. 3 for cross sections of the corresponding processes. For a single layer of microspheres the attenuation of transmitted light intensity is $\Delta I = -I_0 C_{ext} N_S$, where $I_0$ is the input light intensity, $C_{ext}$ is the microparticle extinction cross section and $N_S$ is the particle surface density. Thus $C_{ext} N_S$=1-T, $C_{FS} = FS/N_S$, $C_{BS} = BS/N_S$, and $C_R = R/N_S$, where $C_{ext}$, $C_{FS}$, $C_{BS}$, and $C_R$ are the extinction, forward-scattering, back-scattering, and specular reflection cross sections, respectively. The extinction cross section (black dashed line in Fig. 3) of the gold-coated sphere has decreased as compared to the bare silica microsphere (black solid line)

#250070 Received 14 Sep 2015; revised 8 Oct 2015; accepted 8 Oct 2015; published 12 Oct 2015

near the Mie resonances. Also the forward scattering of the gold-coated spheres (red dashed line) is decreased in average by about 75% compared to the bare silica microspheres (red solid line). The reflectance and backscattering for the gold-coated microspheres have not increased significantly compared to the bare silica microspheres.

**Table 1. Experimental (EXP) and simulations' (SIM) parameters.**

| | Sample #0 | Sample #1 | Sample #2 | Sample #3 | Sample #4 |
|---|---|---|---|---|---|
| Shell thickness, EXP | 0 nm | 43 nm | 63 nm | 67 nm | 67nm |
| Total diameter, EXP | d=785±3nm | d=870±20 nm | d=910±10 nm | d=920±10 nm | d=920±10 nm |
| Total diameter, SIM | 800 nm | 880 nm | 900 nm | 920 nm | 920 nm |
| Plane metal surface coverage (p), EXP | 0 | 0.38±0.03 | 0.47±0.01 | 0.58±0.03 | 0.85±0.02 |
| Metal volume filling factor (f), SIM | 0 | 0.4 | 0.48 | 0.5 | 0.505 |
| Microsphere density number on a substrate, EXP | 0.4±0.02$\mu m^{-2}$ | 0.63±0.07 $\mu m^{-2}$ | 0.66±0.02 $\mu m^{-2}$ | 0.57±0.02 $\mu m^{-2}$ | 0.5±0.02$\mu m^{-2}$ |
| Effective n_sur SIM, | | | | | |
| VIS | 1 | 1.2 | 1.2 | 1.3 | 1.4 |
| IR | 2.4 | 2.4 | 2.4 | 2.4 | 2.4 |
| T @ 560nm, EXP | 29 % | ------ | ------ | ------- | 47 % |
| $C_{FS}$ @ 560nm, EXP | 1.3 $\mu m^2$ | ------- | ------- | ------- | 0.3 $\mu m^2$ |
| Fractal Dimension (D), EXP | | 1.77 | 1.82 | 1.75 | 1.75 |

EXP=experimental values, SIM=values used for simulation, T=transmission, $C_{FS}$=forward scattering cross section, n_sur=refractive index of the surrounding media; VIS=$SiO_2$ substrate, PVP thin coating, and air, IR=ZnSe substrate, PVP, air.

In order to explore the effect of scattering cancelation in the effective medium approximation, numerical simulations have been performed and presented in Fig. 4 for the visible range and infrared range. To calculate the extinction cross section $C_{ext}$ of gold coated silica core-shell particles, we used the Mie theory based algorithm described elsewhere [27]. We modeled the particle as a concentric system with a silica core of radius $r_1$ (400 nm) and gold shell with thickness $t_1$ and total radius $r_2 = r_1 + t_1$. The silica wavelength dependent dielectric constant was taken from [28, 29]. The effective permittivity $\varepsilon_{br}$ of the gold shell in form of semicontinuous film with different metal fraction $f$ was calculated using the Bruggeman effective medium approximation [23].

$$f\frac{\varepsilon_m - \varepsilon_{br}}{\varepsilon_m + 2\varepsilon_{br}} + (1-f)\frac{\varepsilon_h - \varepsilon_{br}}{\varepsilon_h + 2\varepsilon_{br}} = 0 \qquad (1)$$

where $\varepsilon_h$ is the permittivity of host or surrounding medium and $\varepsilon_m$ stands for the Drude-Lorentz model for gold dielectric constant [30]. The filling factor f is from 0 to 1, where 0 corresponds to the case without shell and 1 to a continuous gold film.

The Drude-Lorentz model includes contributions from free electrons and interband transitions: $\varepsilon_m = 1 - \frac{\omega_p^2}{\omega^2 + i\alpha\Gamma_p\omega} + \sum_n \frac{g_n\omega_n^2}{\omega_n^2 - \omega^2 - i\Gamma_n\omega}$. To match the Johnson and Christy (J&C) experimental data [30] we use this equation with Drude parameters $\omega_p = 9\,\mathrm{eV}$, $\Gamma_p = 0.07\,\mathrm{eV}$ [30] and two Lorentzian oscillators with parameters as follows:

#250070 Received 14 Sep 2015; revised 8 Oct 2015; accepted 8 Oct 2015; published 12 Oct 2015

$g_1 = 0.3,\ \omega_1 = 2.7\,\text{eV}, \Gamma_1 = 0.3\,\text{eV}$ , $g_2 = 0.8,\ \omega_2 = 3.05\,\text{eV}, \Gamma_2 = 0.5\,\text{eV}$ [31]. The loss factor $\alpha$ is used to modify the gold damping term ( $\Gamma_p$ ) to introduce the difference between J&C's bulk gold dielectric constant and the dielectric constant of the nanostructured gold. The possible range of the loss factor reported in the literature is from 0.5 for bulk gold [32] and up to 4 for e-beam lithography fabricated nanoparticles [31]. It is known that chemically synthesized nanoparticles have better crystal quality than the continuous thin films, where the grain boundaries contribute in the electron relaxation. This justifies the selection of the loss factor for isolated nanoparticles in the shell to be 0.5-1.

Note that we avoided using the Theye formula for the electron relaxation constant $\Gamma = \tau^{-1} = \tau_0^{-1} + b_\tau \omega^2$ , which is quite popular in the literature on fractal metal films with the parameters involved as fitting in the ranges $\tau_0 = (0.2-3)\times 10^{-15}\,\text{s}$ , $b_\tau = (0.5-3.5)\times 10^{-16}\,\text{s}$ [10,13]. Indeed, such frequency dependence was introduced initially for the electron-electron collisions $\nu_{ee}$ . A careful study of the temperature dependence of the electron relaxation constant by Motulevich proves that $\nu_{ee}$ could only be observed at helium temperatures for metals and spectral ranges, where the interband transitions are negligible [32]. Moreover the assumption of the frequency dependence for the relaxation constant will require frequency dependence of the electron density as well [32], which is hardly expected. The extinction cross section is given by:

$$C_{ext} = \frac{2\pi}{k^2} \sum_{m=1}^{\infty} (2m+1)\,\text{Re}(a_m + b_m) \tag{2}$$

where $k = 2\pi/\lambda$ is the wave vector, $\lambda$ is the wavelength in the ambient medium, and $a_m$ and $b_m$ are the scattering coefficients of electrical field. The coefficients $a_m$ and $b_m$ were calculated using an algorithm described by Wu et al [33]. The sum runs for m from 1 to ∞, but the series can be truncated at some maximum $m_{\max}$ ( $m_{\max} = kr_2$ ) [27]. To closer resemble the experimental conditions in IR spectral range (ZnSe substrate) we used n = 2.4 for the refractive index of surrounding medium.

There are three parameters, which are not known or known with some uncertainty from the experiment. As we mentioned above the plane gold surface coverage p is measured accurately from the SEM images but it should be considered in general as a volume fraction and could be overestimated due to this 3D effect. The shell thickness is measured using the physical boundary of the metal edge, so that the thickness used for the effective permittivity can be less. The effective refractive index of the surrounding medium is estimated as an effective parameter combining contributions of the substrate, PVP coating, and air. It can be coverage dependent and vary from 1.1 to 1.5 for the glass substrate and 1.4 to 2.4 for ZnSe substrate. Thus we use a slight variation of these parameters shown in the Table 1 for best fit of the experimental results.

#250070 Received 14 Sep 2015; revised 8 Oct 2015; accepted 8 Oct 2015; published 12 Oct 2015

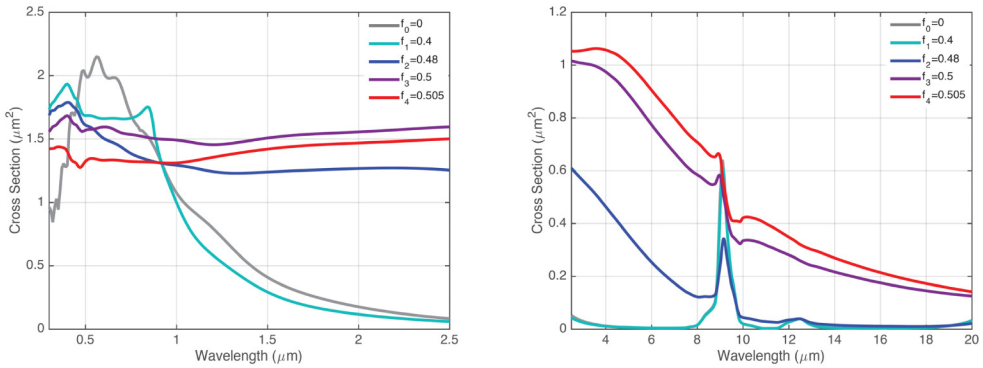


Fig. 4. Extinction cross-section spectra for different metal filling fraction, $f$ (0, 0.4, 0.48, 0.5, and 0.505) simulated for the visible-near IR and IR spectral range.

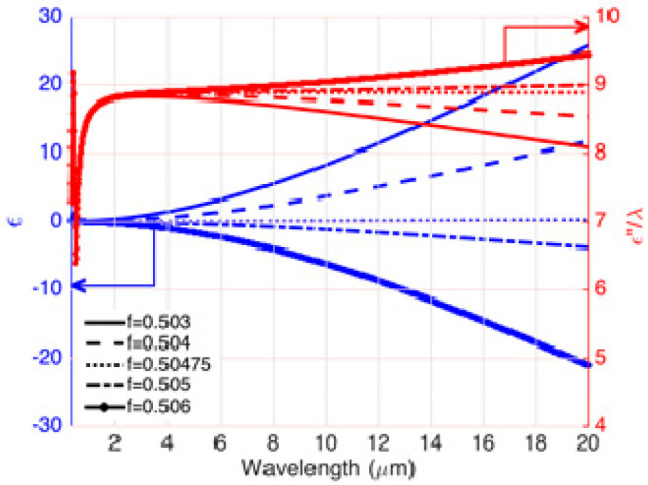


Fig. 5. Real and imaginary effective epsilon of gold film with different metal filling fraction $f$ (0.503, 0.504, 0.50475, 0.505, 0.506).

With the EMT model the simulated optical spectra (Fig. 4) show quite good correspondence to the experimental spectra (Fig. 1). Interestingly the effective permittivity of the shells close to percolation threshold calculated with Eq. (1) shows near zero behavior (Fig. 5) of the real part in the broad spectral range and the product $\omega\varepsilon''$ is weakly dependent (or even independent at $f = 0.50475$) on wavelength. Note that the imaginary part of the permittivity multiplied by the frequency is responsible for the energy density dissipation rate of the monochromatic plane waves. The numerical simulations show that the effective medium model works reasonably well reflecting all the observed features. The model qualitatively reproduces the cancelation of the silica absorption at 9 μm by the gold shell with gradually increasing gold coverage. The model shows also scattering suppression at the Mie resonance wavelength.

The EMT permittivity implies the long-wavelength approximation meaning that the wavelength in the bulk mixture $\lambda_0 / \sqrt{\varepsilon_{eff}}$ is much larger than any scale of the system. It is proven though that the EMT can be inconsistent for the planar films close to the percolation threshold [12,13]. We analyze the limitations of EMT using the scaling theory consideration. The samples can be treated as homogeneous for wavelengths larger than crossover

#250070 Received 14 Sep 2015; revised 8 Oct 2015; accepted 8 Oct 2015; published 12 Oct 2015

wavelength, and the scaling theory reduces to the effective medium description [12]. The scaling theory potentially provides a more general approach to the fractal structure and here we discuss the applicability of EMT using the scaling theory model. In the scaling theory model the relevant length scale $L(\omega)$ is the anomalous diffusion length on the time scale $1/\omega$ ($\omega$ is the optical frequency) and can be much shorter than the optical wavelength. As long as the percolation correlation length $\xi$ is larger than length scale $L(\omega)$, the film is inhomogeneous and the effective-medium approach is not applicable. Following the above arguments, films close to the percolation threshold may appear inhomogeneous even in the far-infrared regime, where $\xi$ is much shorter than the optical wavelength but larger than $L(\omega)$. According to Yagil et al. [13] $L(\omega) = L_0\xi_0(1/k\xi_0)^{1/(2+\theta)}$, where $k$ is the wavenumber, $\theta = 0.8$ for 2D, $L_0$ is a coefficient of about unity, and $\xi_0$ is the characteristic scale of the percolation correlation length. The exponent $\nu$ determines the scaling behavior of the percolation correlation length as $p$ approaches $p_c$, $\xi = \xi_0\left[(p-p_c)/p_c\right]^{-\nu}$. The crossover from inhomogeneous to homogeneous behavior occurs at the wavelength $\lambda_\xi = 2\pi\xi_0(\xi/L_0\,\xi_0)^{2+\theta}$. Using the literature data [13] with $\xi_0 = 10\,\text{nm}$, $L_0 = 1$ [10], $p_c = 0.68$, $\nu = 1.33$, we obtained the crossover wavelength of 370 nm at p = 0.505. The other source data [13] gives $L_0 = 4$ resulting in the crossover wavelength about 8 nm at p = 0.505. Our simulations use p = 0.505 and the whole spectral range can be well described by the effective medium theory. This explains why the EMT shows quite good agreement with the experimental results. Note also that the long-wavelength condition, where the wavelength in the bulk mixture $\lambda_0/\sqrt{\varepsilon_{eff}}$ is much larger than any scale of the system, is fulfilled due to the epsilon-near-zero effective permittivity.

## 3. Methods

In order to fabricate core- fractal shell microspheres we modified a recipe developed for continuous shells [24]. Specifically, 30 mg of potassium carbonate ($K_2CO_3$) has been dissolved in 100mL of ultra-pure water, the solution was stirred for 10 minutes, and 300 μL of 50 mM $HAuCl_4$ was added in the solution. Next, about $8x10^8$ of the amine functionalized silica microspheres and then 40μL of 0.36 mM $CH_2O$ were added to the solution and vigorously stirred. After the growth of the gold shells, the solution was stabilized with polyvinylpyrrolidone (PVP) to prevent aggregation of the microspheres. Finally, the solution was centrifuged to collect gold-coated silica microspheres. Collected particles were again dispersed several times in ultra-pure water in order to remove remaining excess of constituents. The synthesized gold-coated microspheres were deposited on zinc selenide (ZnSe) substrates for the infrared spectroscopy and on fused silica substrates for spectroscopy in the visible range. Silica microspheres were purchased from Bangs Laboratories, Inc. All other chemicals, PVP, $HAuCl_4$, $K_2CO_3$, and $CH_2O$ were purchased from Sigma-Aldrich.

The structural characterization was performed with Hitachi S-4800 field emission scanning electron microscope (FESEM). To collect the optical spectra in 0.32μm-2.5μm and 2.5μm-20μm wavelength ranges, we used Perkin Elmer Lambda 950 spectrometer and Nicolet Fourier-transform infrared (FTIR) Nexus 670 spectrometer, respectively. The reflectance and scattering measurements were performed with the integrating sphere module of the Perkin Elmer Lambda 950 spectrometer [25].

## 4. Conclusions

Our experiments show that the optical response of the core-shell microsphere with a gold fractal shell is dominated by the shell absorption. Similar to the planar fractal films, the

#250070 Received 14 Sep 2015; revised 8 Oct 2015; accepted 8 Oct 2015; published 12 Oct 2015

absorption is enhanced in the broad spectral range up to 20 μm . It is interesting though that the specular reflection and backscattering are relatively small for the fractal shells due to 3D spherical geometry. What is also counterintuitive is that the resulting transmission cross-section for the core-shell is higher than the bare silica core at the Mie resonance. This is however due to the forward scattering suppression of silica microspheres by adding the plasmonic gold shells. Increasing the gold coverage can gradually decrease the scattering peak of silica microsphere in the visible range, where the microsphere size is greater than wavelength. By measuring transmittance, reflectance, and forward- and back- scattering we found that the absorption in the shell contributes the most to the extinction of the whole core-shell microsphere. Another surprising result is that the Mie scattering resonance at 560 nm of a silica core with 780 nm diameter is suppressed by 75% and partially substituted by the absorption in the shell so that the total transmission is increased by factor of 1.6 due to the gold fractal shell. The effective permittivity of the gold shell manifests the epsilon-near-zero condition over the whole spectral range under study. Also, in the mid infrared spectral range, one can see that the Si-O-Si vibrational stretching band of the core is “hidden” in the spectra of the core-shell extinction. As the gold coverage increases on the silica microspheres, the relative contribution of the vibrational stretching band at 9 μm in the total extinction is gradually decreasing and finally disappears. Effective medium theory describes the experimental spectra reasonably well and gives an epsilon-near-zero real part of the effective shell permittivity and approximately wavelength independent product of the imaginary part of the permittivity and light frequency over the broad spectral range 0.5-20 μm (this product is responsible for the energy density dissipation rate of the plane wave).These observations for the visible and mid-IR spectra indicate that the light goes mostly through the epsilon-near-zero shell with approximately wavelength independent absorption rate. Thus the fractal films being synthesized on the microspheres show interesting properties of ”guiding” light and could be promising aerosolized obscurants in the visible-infrared spectral range.

**Acknowledgments**

Authors thank M. Segev and V.M. Shalaev for helpful discussions. This work was partially supported by the U.S. Army Research Office grant W911NF-11-1-0333. PN thanks for support by the Polish Ministry of Science and Higher Education grant OR00005408.

#250070 Received 14 Sep 2015; revised 8 Oct 2015; accepted 8 Oct 2015; published 12 Oct 2015